Effect of Periodic Accelerations on Interface Stability in a Multilayered Fluid Configuration

M. J. Lyell* and Michael Roh†
West Virginia University, Morgantown, West Virginia 26505

The increasing number of research opportunities in a microgravity environment will benefit not only fundamental studies in fluid dynamics, but also technological applications such as those involving materials processing. In particular, fluid configurations that involve fluid-fluid interfaces would occur in a variety of experimental investigations. This work investigates the stability of a configuration involving fluid-fluid interfaces in the presence of a time-dependent (periodic) forcing. The fluid configuration is multilayered and infinite in extent. The analysis is linear and inviscid, and the acceleration vector is oriented perpendicular to each interface. A Floquet analysis is employed, and the resulting algebraic eigensystem is truncated. Nondimensional parameters appear in the algebraic system. A numerical study is performed to elucidate the regions of instability and the effect of parameter variation on the fluid configuration stability.

Nomenclature

$\underline{A},\underline{B}$ = matrices representing final system
$A(t)$ = time-dependent coefficient, nondimensional
Bo = nondimensional parameter, = $(\rho_{av}H^2G_o/\gamma)$
Fe = equilibrium interface, nondimensionalized
Fr = nondimensional parameter, = $[G_o/(H\omega_f^2)]$
G_o = peak value of forcing, dimensional
$g(t)$ = forcing term, nondimensionalized
H = height of middle slab, dimensional
k = wave number of perturbation, nondimensional
$\hat{\boldsymbol{n}}$ = outward pointing unit normal to interface
p = pressure field, nondimensionalized
$\boldsymbol{u}$ = velocity field, nondimensionalized
t = time, nondimensionalized
γ = surface tension
λ = Floquet exponent, eigenvalue
ρ = density
ϕ = velocity potential, nondimensionalized
ω_f = frequency of periodic acceleration (forcing)

Subscripts

I = (finite) middle layer fluid region of height H
II = upper layer (unbounded) fluid region
III = lower layer (unbounded) fluid region
2 = upper interface
3 = lower interface

Superscripts

$\dot{(\,)}$ = differentiation
$\hat{(\,)}$ = unit vector (e.g., $\hat{e}_x$, $\hat{e}_y$, $\hat{e}_z$, $\hat{\boldsymbol{n}}$ or part of vector definition (e.g., $\hat{\boldsymbol{x}}$)
$\tilde{(\,)}$ = dimensional quantities

Received Aug. 27, 1990; revision received Dec. 6, 1990; accepted for publication Jan. 28, 1991.

*Assistant Professor, Mechanical and Aerospace Engineering Department, Box 6101. Senior Member AIAA.
†Graduate Student, Mechanical and Aerospace Engineering Department, Box 6101.

Introduction

CURRENT interest in microgravity materials processing has focused attention upon certain relevant aspects of fluid mechanics in this environment. In particular, a number of materials processing applications involve fluid-fluid interfaces.

The environment onboard the Space Shuttle is not strictly a microgravity environment. Rather, residual accelerations exist that could affect any ongoing materials science or space processing experiments. A recent summary[1] indicates that accelerations include those in the frequency range of <10 Hz, with acceleration levels ranging from $10^{-6}\,g_{\text{earth}}$ to $10^{-3}\,g_{\text{earth}}$. In addition to periodic forcing, residual accelerations may be of impulse type, due to such causes as stationkeeping maneuvers and astronaut motion.[2]

This work investigates the effect of periodic accelerations on the interface stablity of an idealized fluid configuration. The fluid configuration is multilayered and infinite in extent (see Fig. 1). The accelerations are periodic about a zero mean g level and are oriented normal (in the $\hat{e}_z$ direction) to each interface.

Previous work has investigated the stability of a single planar free surface subject to periodic forcing in the direction perpendicular to the interface.[3,4] These studies were both done

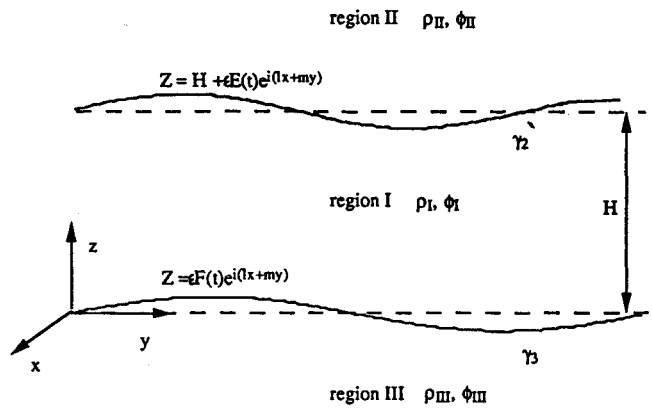

Fig. 1 Multilayer fluid configuration geometry schematic.

in a terrestrial environment and required the use of a container. In the work of Benjamin and Ursell,[3] the container was cylindrical in shape. Their analysis resulted in a Mathieu equation that governed the time-dependent amplitude of the disturbance. They were able to make statements concerning the interface stability based on known mathematical properties of Mathieu equations. The case of a rectangular container has been addressed recently,[4] and the results extended into the nonlinear regime. Both of these investigations utilized an inviscid analysis.

The effect of viscosity on the stability properties has been studied recently in idealized infinite or semi-infinite configurations that had one fluid-fluid interface.[5,6] Again, the periodic forcing was directed normal to the interface. One theoretical investigation was done assuming a zero mean g level and pertains to the microgravity environment.[6] Results were obtained for different regions of parameter space, and some stability boundaries were determined.

The present work will study the stability of an idealized multiple-layer fluid configuration that is infinite in the $\hat{e}_x$ and $\hat{e}_y$ directions (as well as unbounded in the $\hat{e}_z$ direction) and is subjected to periodic forcing normal to each interface. The height of the middle layer is finite. In general, the densities in each region differ, as do the surface tension values at the upper and lower interfaces. The analysis is linear and inviscid. A Floquet analysis is employed. Details of the analysis are presented in the next section.

The configuration is idealized, as was the case in previous work. However, the use of nondimensional parameters in the stability investigation will enable trends to be discerned and parameter regions (of instability) to be identified.

Equation Development

Governing Equations

The governing equations are those of conservation of mass and momentum applied to an inviscid and incompressible fluid, and are

$$\tilde{\nabla} \cdot \tilde{u} = 0 \tag{1}$$

$$\tilde{\rho}\left\{\left(\frac{\partial \tilde{u}}{\partial \tilde{t}}\right) + \tilde{u} \cdot \tilde{\nabla}\tilde{u}\right\} = -\tilde{\nabla}\tilde{p} - \tilde{\rho}\tilde{G}_o g(\omega_f \tilde{t})\,\hat{e}_z \tag{2}$$

The time-dependent body force term is indicated in Eq. (2). G_o represents the peak value of the acceleration due to the periodic forcing. The function $g(\omega_f t)$ is periodic and will be taken to be a cosine function. The fluid system is linearized about a state of zero mean motion, and quadratically small terms (after expansion in a small parameter ε) are neglected. Use of nondimensionalizations

$$\tilde{x} = H\,x, \qquad \tilde{t} = \omega_f^{-1}\,t \tag{3a}$$

$$\tilde{u} = H\omega_f\,u, \qquad \tilde{p} = \rho_{av} H^2 \omega_f^2\,p \tag{3b}$$

yields

$$\nabla \cdot u = 0 \tag{4}$$

$$\left(\frac{\rho}{\rho_{av}}\right)\left\{\frac{\partial u}{\partial t}\right\} = -\nabla p - \left(\frac{\rho}{\rho_{av}}\right)\left(\frac{G_o}{H\omega_f^2}\right) g(t)\,\hat{e}_z \tag{5}$$

The parameter $Fr = (G_o/H\omega_f^2)$ is taken to be roughly of order 1. Note that the mean pressure field will be periodic in time. (Also, p is expanded into both a mean and perturbation contribution.) A potential function ϕ with $u = \nabla\phi$, is defined. Substitution into Eq. (4) yields Laplace's equation. Perturbations are taken to be wavelike in the (xy) plane. That is, they are oscillatory. The resulting differential equations (in z) are solved in the middle, upper, and lower regions to yield

$$\phi_{\mathrm{I}} = \{A(t)\exp(kz) + B(t)\exp(-kz)\}\exp(i[lx + my]) \tag{6a}$$

$$\phi_{\mathrm{II}} = \{C(t)\exp(-kz)\}\exp(i[lx + my]) \tag{6b}$$

$$\phi_{\mathrm{III}} = \{D(t)\exp(kz)\}\exp(i[lx + my]) \tag{6c}$$

Note that A, B, C, and D are time-dependent coefficients. The wave number k is given by $\sqrt{(l^2 + m^2)}$.

Equations representing the upper and lower equilibrium interfaces are

$$Fe_2 = z - 1 - \varepsilon\,E(t)\exp(i[lx + my]) \tag{7}$$

$$Fe_3 = z - \varepsilon\,F(t)\exp(i[lx + my]) \tag{8}$$

Note that E and F are time-dependent coefficients. Thus, for example, the functional form of the perturbation to the mean interface at $z = 0$ is given by the expression $E(t)\exp(i[lx + my])$. At this stage, the time-dependent coefficients are unknowns.

Boundary Conditions

The kinematic condition, which holds at each interface, requires that

$$\left(\frac{\partial Fe}{\partial t}\right) + u \cdot \nabla Fe = 0 \tag{9a}$$

After linearization, only the u_z velocity component will contribute. This results in

$$\dot{E}(t) + k\,C(t)\,e^{-k} = 0 \qquad \text{on} \quad z = 1 \tag{9b}$$

$$-\dot{F}(t) + k\,D(t) = 0 \qquad \text{on} \quad z = 0 \tag{9c}$$

In addition to the kinematic condition, the normal component of the velocity is continuous across an interface, which yields

$$\left(\frac{\partial \phi_{\mathrm{I}}}{\partial z}\right) = \left(\frac{\partial \phi_{\mathrm{II}}}{\partial z}\right) \qquad \text{on} \quad z = 1 \tag{10a}$$

$$\left(\frac{\partial \phi_{\mathrm{I}}}{\partial z}\right) = \left(\frac{\partial \phi_{\mathrm{III}}}{\partial z}\right) \qquad \text{on} \quad z = 0 \tag{10b}$$

or

$$A(t)\,e^{2k} - B(t) = -C(t) \qquad \text{on} \quad z = 1 \tag{10c}$$

$$A(t) - B(t) = D(t) \qquad \text{on} \quad z = 0 \tag{10d}$$

The remaining boundary condition is the (linearized) normal force balance across an interface. In nondimensional form, it is

$$(Bo/Fr)\,(\Delta p) = \nabla \cdot \hat{n} \tag{11}$$

The unit vector $\hat{n}$ is the linearized outward pointing normal to the interface. After substitution, Eq. (11) yields

$$\{([\rho_{\mathrm{II}} - \rho_{\mathrm{I}}]/\rho_{av})\,Fr\,g(t)\,E(t) - (\rho_{\mathrm{I}}/\rho_{av})[\dot{A}(t)e^{k} + \dot{B}(t)e^{-k}] + (\rho_{\mathrm{II}}/\rho_{av})\dot{C}(t)e^{-k}\} = (Fr/Bo_2)\,k^2\,E(t) \qquad \text{on} \quad z = 1 \tag{12a}$$

$$\{([\rho_{\mathrm{I}} - \rho_{\mathrm{III}}]/\rho_{av})\,Fr\,g(t)\,F(t) + (\rho_{\mathrm{I}}/\rho_{av})[\dot{A}(t) + \dot{B}(t)] - (\rho_{\mathrm{III}}/\rho_{av})\dot{D}(t)\} = (Fr/Bo_3)\,k^2\,F(t) \qquad \text{on} \quad z = 0 \tag{12b}$$

with

$$Bo_2 = (\rho_{av} H^2 G_o/\gamma_2)$$
$$Bo_3 = (\rho_{av} H^2 G_o/\gamma_3)$$
$$Fr = G_o/(H\omega_f^2)$$

The term $\gamma_2(\gamma_3)$ indicates the surface tension at the upper (lower) interface.

Final System of Equations

Through the utilization of Eqs. (10c) and (10d), the $C(t)$ and $D(t)$ coefficients can be eliminated to yield the following system:

$$\dot{A}(t)\{-3(1+\rho_{21})/(1+\rho_{21}+\rho_{31})\}e^k + \dot{B}(t)\{3(\rho_{21}-1)/(1+\rho_{21}+\rho_{31})\}e^{-k} + E(t)\{3(\rho_{21}-1)/(1+\rho_{21}+\rho_{31})\}Fr\,g(t) = (Fr/Bo_2)\,k^2\,E(t) \quad (13a)$$

$$\dot{A}(t)\{3(1-\rho_{31})/(1+\rho_{21}+\rho_{31})\} + \dot{B}(t)\{3(1+\rho_{31})/(1+\rho_{21}+\rho_{31})\} + F(t)\{3(1-\rho_{31})/(1+\rho_{21}+\rho_{31})\}Fr\,g(t) = (Fr/Bo_3)\,k^2\,F(t) \quad (13b)$$

$$\dot{E}(t) = k\{A(t)\,e^k - B(t)e^{-k}\} \quad (13c)$$

$$\dot{F}(t) = k\{A(t) - B(t)\} \quad (13d)$$

with $\rho_{21} = (\rho_{II}/\rho_I)$ and $\rho_{31} = (\rho_{III}/\rho_I)$.

The governing system of equations has been reduced to four ordinary differential equations (in time) with nonconstant coefficients and with four unknowns. It remains to determine the stability of this system for various values of the parameters Fr, Bo_2, Bo_3, ρ_{21}, ρ_{31}, and k. As was mentioned previously, $g(t)$ is chosen to be $\cos(t)$.

Floquet theory[7] can be applied to system (13). Let the time-dependent coefficients be expressed as

$$\{A(t),B(t),E(t),F(t)\} = \sum_{n=-\infty}^{\infty}\{A_n,B_n,E_n,F_n\}\,e^{int}e^{\lambda t} \quad (14)$$

The system of four ordinary differential equations in time is now re-expressed as an infinite algebraic system, with the Floquet exponent appearing as another parameter. That is,

$$e^k(\lambda+in)\{-3(1+\rho_{21})/(1+\rho_{21}+\rho_{31})\}A_n + e^{-k}(\lambda+in)\{3(\rho_{21}-1)/(1+\rho_{21}+\rho_{31})\}B_n - (Fr/Bo_2)k^2E_n + \{3(\rho_{21}-1)/(1+\rho_{21}+\rho_{31})\}(Fr/2)(E_{n-1}+E_{n+1}) = 0 \quad (15a)$$

$$(\lambda+in)\{3(1-\rho_{31})/(1+\rho_{21}+\rho_{31})\}A_n + (\lambda+in)\{3(1+\rho_{31})/(1+\rho_{21}+\rho_{31})\}B_n - (Fr/Bo_3)k^2F_n + \{3(1-\rho_{31})/(1+\rho_{21}+\rho_{31})\} \times (Fr/2)(F_{n-1}+F_{n+1}) = 0 \quad (15b)$$

$$(\lambda+in)E_n + ke^{-k}B_n - ke^kA_n = 0 \quad (15c)$$

$$(\lambda+in)F_n + kB_n - kA_n = 0 \quad (15d)$$

The value of n varies from $-\infty$ to ∞. The infinite set of homogeneous equations can be written in matrix form as

$$\{\underline{B}^{-1}(\underline{A}) - \lambda\,\underline{I}\}\,\hat{x} = \mathbf{0} \quad (16a)$$

or

$$\underline{A}\,\hat{x} = \lambda\,\underline{B}\,\hat{x} \quad (16b)$$

The latter representation is in the form of a generalized eigenvalue problem. The Floquet exponent λ serves as the eigenvalue. The infinite column vector $\hat{x}$ contains $(A_n,B_n,E_n,F_n)^T$. For details concerning the form of matrices $\underline{A}$ and $\underline{B}$, and column vector $\hat{x}$, see the Appendix.

The sign on the Floquet exponent/eigenvalue λ indicates the stability. If λ is a positive value, then the disturbance will grow and the interface configuration will be unstable. As this is a linear analysis, no information can be obtained concerning the finite amplitude (nonlinear) form of the configuration. Numerical methods are used to determine the value of λ for different values of the parameters. These are discussed in the next section along with various results.

Results

Comments on Numerical Method

The linear algebraic system given by Eqs. (16) is truncated. Results are presented for a truncation value of $n = |25|$, which involves a system of 204 equations. This resulting system forms a generalized eigenvalue problem, with the matrices $\underline{A}$ and $\underline{B}$ having complex entries. At this level of truncation, both $\underline{A}$ and $\underline{B}$ are sparse.

Eigenvalue techniques were used to determine λ values. An IMSL routine (DGVLCG), based on an LZ algorithm,[8] was utilized. In particular, we are interested in the value of the largest Real(λ), which gives the fastest growing mode. If Real(λ) is positive, the perturbation is growing exponentially. Hence, the fluid configuration is then unstable with respect to the perturbations in the presence of the unsteady periodic acceleration (forcing) field.

Several checks were made to insure that the eigenvalues obtained were correct. Higher truncations yielded the same largest Real(λ) value. As an additional check, the generalized eigenvalue problem was reformulated as a standard eigenvalue problem of the form $(\underline{B}^{-1}\underline{A} - \lambda\,\underline{I})\,\hat{x} = \mathbf{0}$ and the eigenvalues of this new system were determined. This was done by utilizing an alternate IMSL routine (DEVLCG) based on a different numerical algorithm. Again, the values of Real(λ) were in agreement with those obtained previously. As a final check, a limit case was run (for various parameter values). The value of Bo_2 was set to infinity, which is equivalent to setting the surface tension at the upper interface to zero. In addition, the densities in regions I and II were set to the same value. This limit case represents the one interface case. The actual one interface case was developed separately. Results obtained from using the two interface system (and code developed for it) in the aforementioned limit case and from solving directly the one interface system agreed quite closely.

Discussion of Results

A parametric study was performed to investigate the effects of variation in Bo_2, Bo_3, Fr, and the density ratios with wave number. Because of space limitations, a subset of results that were obtained are presented. (These are illustrative and typical.) In each case, if the periodic forcing function $g(t)$ were to be set to zero, and with the mean gravity level zero, the configuration would be stable to the wave-type small amplitude disturbances. That is, the interface would simply oscillate. It is only with the forcing, and in the indicated parameter regions, that instability does result.

The values of the wave numbers vary between 0.10 and 5.00. Although not all results are presented, the investigation

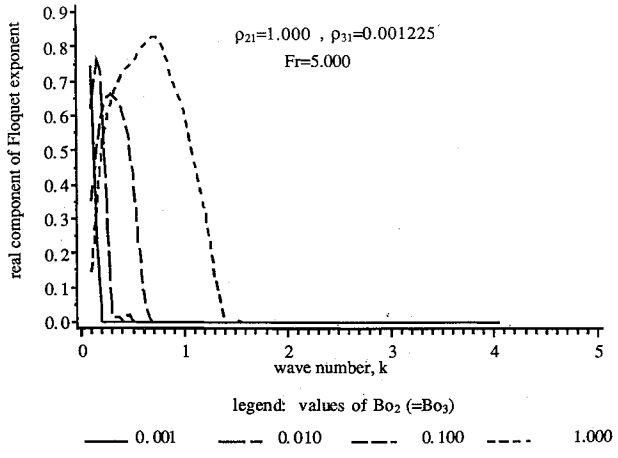

Fig. 2 Effect of *Bo* on stability: $\rho_{21} = 1.00$; $\rho_{31} = 0.001225$; $Fr = 5.00$.

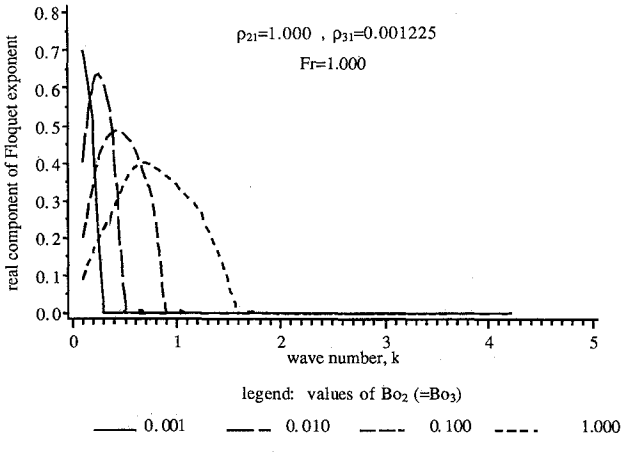

Fig. 3 Effect of *Bo* on stability: $\rho_{21} = 1.00$; $\rho_{31} = 0.001225$; $Fr = 1.00$.

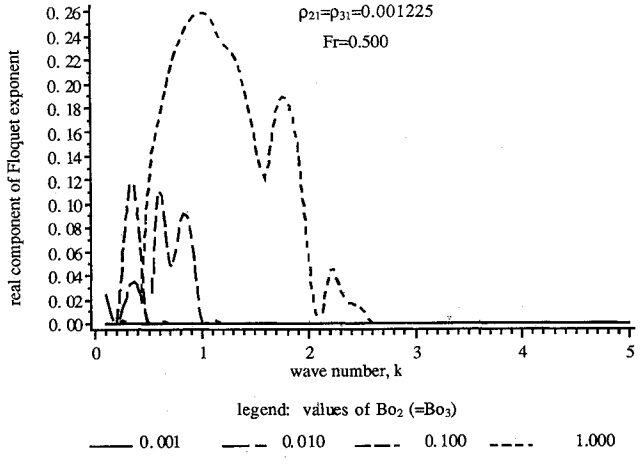

Fig. 4 Effect of *Bo* on stability: $\rho_{21} = \rho_{31} = 0.001225$; $Fr = 0.50$.

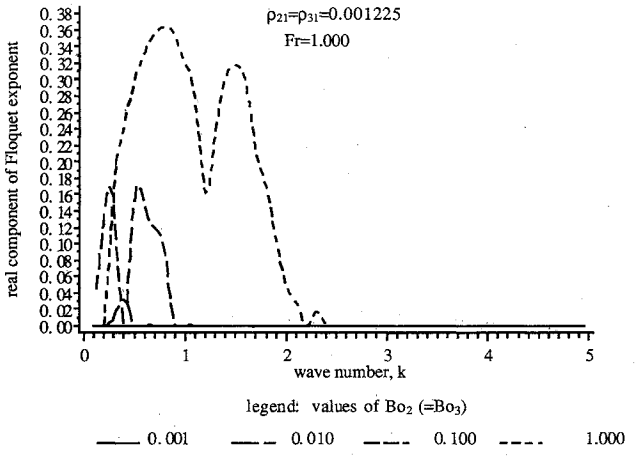

Fig. 5 Effect of *Bo* on stability: $\rho_{21} = \rho_{31} = 0.001225$; $Fr = 1.00$.

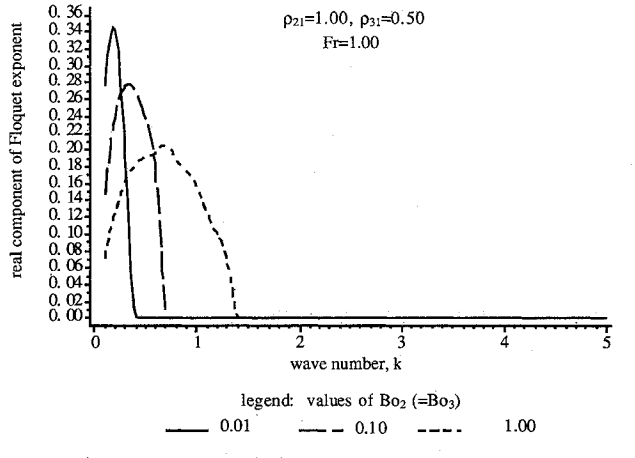

Fig. 6 Effect of *Bo* on stability: $\rho_{21} = 1.00$; $\rho_{31} = 0.50$; $Fr = 1.00$; $Bo_3 = Bo_2$.

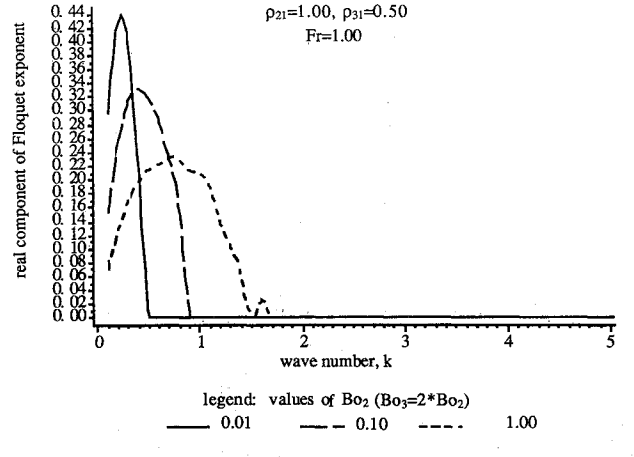

Fig. 7 Effect of *Bo* on stability: $\rho_{21} = 1.00$; $\rho_{31} = 0.50$; $Fr = 1.00$; $Bo_3 = 2 \times (Bo_2)$.

considered Bo_2 values of (1.0, 0.1, 0.01, 0.001). The values of Bo_3 were set equal to Bo_2, or were twice those of Bo_2 in different studies.

Figures 2–10 show graphs of Real(λ) vs wave number for various values of Bo_2, Bo_3, Fr, ρ_{21}, and ρ_{31}. Note that Real(λ) is the largest eigenvalue and represents the fastest growing (unstable) wave if positive. Regions for which Real(λ) ≤ 0 are indicated by being set equal to zero in the graphs. That is, the value of Real(λ) < 0 is not of interest.

In Figs. 2–7, the effect of Bo_2 and Bo_3 on stability for different Fr and density ratos is elucidated. In Fig. 2, Bo_2 is set equal to Bo_3 for the density ratios $\rho_{21} = 1.0$ and $\rho_{31} = 0.001225$ and for $Fr = 5.00$. The unstable wave number region is broadest for the largest $Bo_2(Bo_3)$ values. As $Bo_2(Bo_3)$ is decreased, the unstable wave number region shrinks to encompass fewer k values and tends toward the lower k region. For low $Bo_2(Bo_3)$ values, this two interface configuration is unstable to the longer wavelength disturbances in the presence of periodic forcing. The effect of a decrease in Fr, keeping the other parameter values the same, is seen in Fig. 3. The range of unstable wave numbers broadens, with smaller wavelengths falling into the unstable region.

The density ratios indicated in Figs. 4 and 5 pertain to a gas-liquid-gas configuration. As was the situation in the preceding two figures, the broadest range of unstable wave number values occurs for the largest $Bo_2(Bo_3)$ value. As Fr is decreased, the unstable wave number band encompasses larger values (corresponding to smaller wavelength disturbances). Inspection of Fig. 5 shows a slight separation in unstable wave number bands near $k = 2.175$. This k value falls into an unstable region at the smaller Fr value given in Fig. 4. Note that the configuration represented in Figs. 4 and 5 is stable when $Bo_2(Bo_3)$ is 0.001. That is, Real(λ) > 0 only for the larger $Bo_2(Bo_3)$ values in the indicated k ranges.

The effect of Bo_2 not equal to Bo_3 on the configuration stability is shown in Figs. 6 and 7 (for the given values of Fr and density ratios). In Fig. 6, the Bo values are equal. This is changed in Fig. 7, with Bo_3 twice Bo_2. Physically, the increase of Bo_3 while keeping Fr fixed can be interpreted as a change (decrease) in the surface tension value at the lower interface. The predominant effect is to broaden the range of unstable wave numbers for each set of Bo_2, Bo_3 values. Note that the numerical value of the real part of the Floquet exponent λ is increased for Bo_3 twice the value of Bo_2, indicating a faster growing "fastest growing" disturbance at the lower Bo_2 values.

In Fig. 8, the effect of holding the (Bo_2,Bo_3) values fixed (for the specified density ratios) and varying Fr is shown. As Fr is decreased, the range of unstable wave numbers increases. Physically, this can be interpreted as a decrease in configuration stability with respect to the wavelike disturbances for somewhat larger frequencies of the periodic forcing.

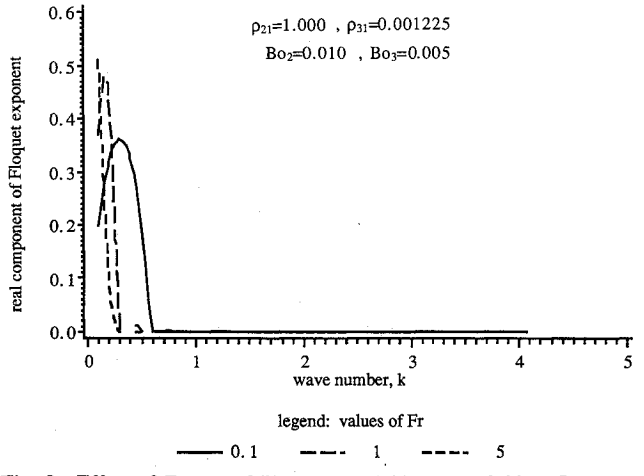

Fig. 8 Effect of Fr on stability: $\rho_{21} = 1.00$; $\rho_{31} = 0.001225$; $Bo_2 = 0.01$; $Bo_3 = 0.005$.

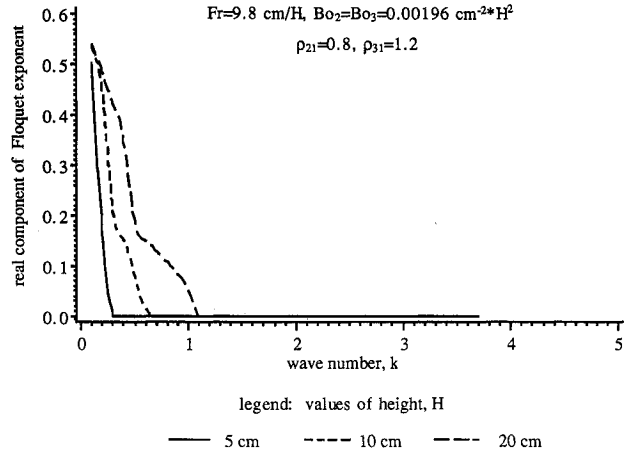

Fig. 9 Effect of height variation: $Fr = 9.8$ cm/H; $Bo_2 = Bo_3 = 0.00196 \times H^2cm^{-2}$; $\rho_{21} = 0.80$; $\rho_{31} = 1.20$.

The height of the finite middle slab is a physical quantity that appears in both the Bo and Fr nondimensional parameters. In particular, Fr is inversely proportional to the height, whereas Bo depends on the square of the height. An increase in height H implies a decrease in Fr and an increase in Bo. As was seen in Figs. 2–7, the region of instability in wave number space becomes larger as Bo increases. From Fig. 8, it is seen that the broadest region of instability (with respect to k) corresponds to the smallest Fr values. It is anticipated that an increase in H will result in an unstable configuration for a broader range of k values. This is borne out in Fig. 9. Results are presented graphically for the case $G_o = (10^{-4}\ g_{earth})$, $\omega_f = 0.1$ Hz, and $\gamma_2 = \gamma_3 = 50$ dynes/cm. In addition, $\rho_{21} = 0.8$ and $\rho_{31} = 1.2$.

The effect of density ratio difference on stability is presented in Fig. 10. Values of ρ_{21} and ρ_{31} represent the density ratios of the upper and lower regions to that of the middle layer, respectively. Among cases indicated, the largest magnitude difference in the density ratios is $(\rho_{31} - \rho_{21} = 9)$. This corresponds to the case having the largest range of unstable wave numbers. Note that all three cases belong to a family with $\rho_{21} = 1.0$. In addition, the case in which both density ratios were set to 1, indicating equal densities in all three regions, was addressed. Under the action of periodic forcing, lack of density differences among the layers results in lack of instability.

The wave number at which the subharmonic occurs is plotted in Fig. 11 for a range of Fr values at the indicated Bo values and density ratios. It is seen that there is a shift of the subharmonic to lower wave numbers as Fr increases, i.e., as the forcing frequency decreases.

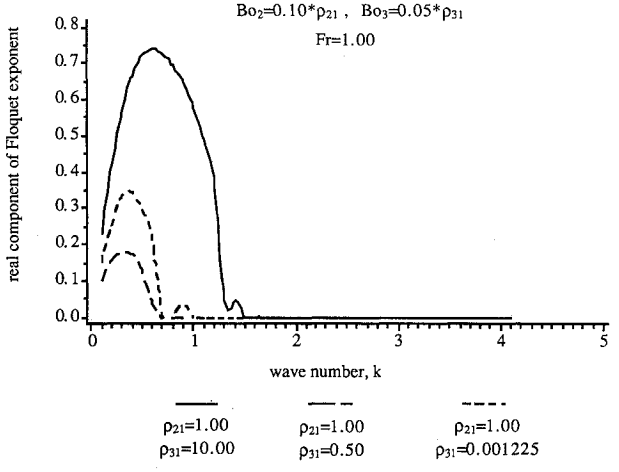

Fig. 10 Effect of density ratios on stability: $Bo_2 = 0.10 \times \rho_{21}$; $Bo_3 = 0.05 \times \rho_{31}$; $Fr = 1.00$.

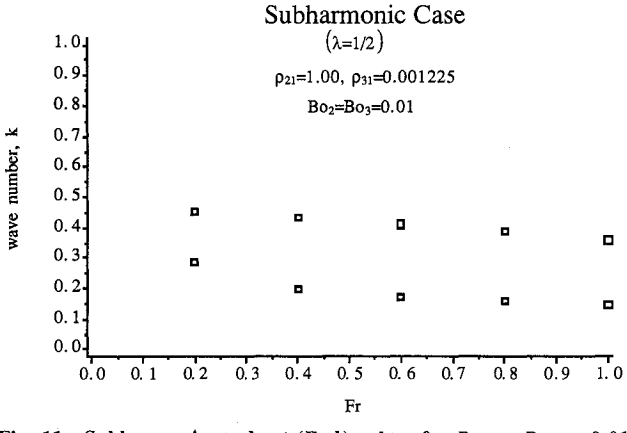

Fig. 11 Subharmonic mode at (Fr,k) values for $Bo_2 = Bo_3 = 0.01$: $\rho_{21} = 1.00$; $\rho_{31} = 0.001225$.

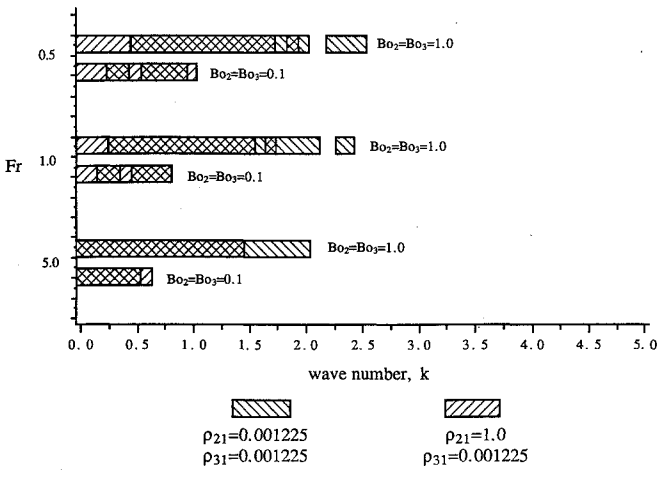

Fig. 12 Stability boundaries: cases $\rho_{21} = \rho_{31} = 0.001225$; and $\rho_{21} = 1.00$, $\rho_{31} = 0.001225$.

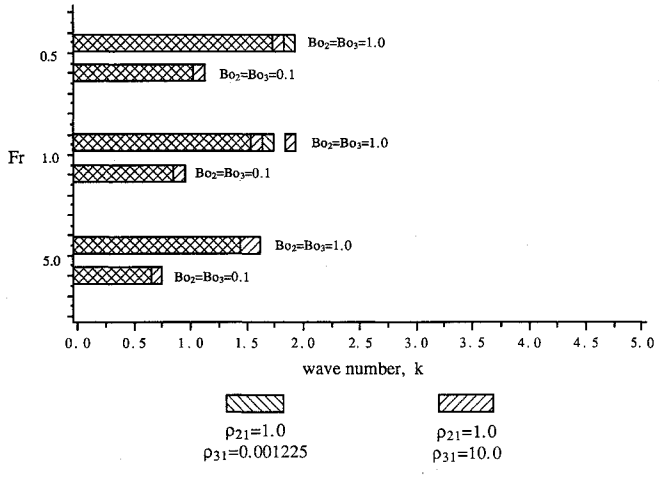

Fig. 13 Stability boundaries: cases $\rho_{21} = 1.00$, $\rho_{31} = 10.00$; and $\rho_{21} = 1.00$, $\rho_{31} = 0.001225$.

Stability boundaries of Fr vs k are plotted in Figs. 12 and 13. (Recall that Fr is inversely proportional to the square of ω_f.) This is done for configurations of different density ratios (as indicated by the different area fill patterns). Moreover, on each graph, multiple values of Bo_2,Bo_3 are represented. The unstable regions are indicated by the rectangular filled regions. No meaning is ascribed to the width of the rectangles.

Conclusions

The effect of periodic accelerations on the stability of a multilayered, two interface, unbounded fluid system has been studied using Floquet analysis. In addition to the wave number, five parameters appear in the problem: Bo_2, Bo_3, Fr, ρ_{21}, and ρ_{31}. Fr is inversely proportional to the square of the forcing frequency, and $Bo_2(Bo_3)$ is inversely proportional to $\gamma_2(\gamma_3)$.

Several trends were discerned in the parameter study. For fixed density ratios ρ_{21} and ρ_{31}, as well as fixed Fr, the range of unstable wave numbers increases as $Bo_2(Bo_3)$ increases. If it is only the parameter Fr that is varied, it is found that the range of unstable wave numbers increases as Fr is decreased. (Note that the variation in Fr values is very limited.) Physical interpretation of these trends has been presented in the preceding section.

Although the comparison is not presented graphically, the multilayered fluid system was found to be, in general, more unstable than the one interface fluid configuration. That is, the range of unstable wave numbers is smaller in the one interface case. In particular, the greatest contrast was in the low k region. This conclusion was determined through consideration of a limit case that involved setting Bo_3 to infinity and ρ_{31} to 1 in order to study the effect of having only one interface using the code developed for the two interface configuration. In this way, the parameters are consistent in both problems.

In the stability boundary diagrams of Figs. 12 and 13, the rectangular filled regions indicate instability. It is clear that, over the indicated range of $Bo_2(Bo_3)$ and Fr values, the configuration is generally unstable at lower wave numbers ($k < 1$). An exception is the gas-liquid-gas configuration ($\rho_{21} = \rho_{31} = 0.001225$) at lower Fr values. Note also that the regions of instability are punctuated by stable regions for the range of Bo values and all but the highest Fr value.

The configuration used in this study was idealized. In an actual space processing application, the fluid configuration would not be infinite in extent. Boundary conditions pertinent to the specific application would have to be taken into account. Nevertheless, the results obtained in this study can be used in a qualitative manner when considering a specific materials processing geometry.

For example, it has been determined that the multilayered fluid system is, in general, unstable over a broader range of k values than the one interface fluid configuration. This has implications for a float zone processing technique in which the fluid cylinder is multilayered. Also, the investigation into the important subharmonic case shows that it occurs at wave numbers that increase with decreasing Fr values. That is, in the more unstable Fr range, the subharmonic (Floquet exponent $\lambda = \frac{1}{2}$) will occur at smaller values of the perturbation wavelength. A materials processing fluid configuration then could be susceptible to instability due to small wavelength fluctuations in the presence of periodic forcing. The nondimensional idealized system has been studied over the range of parameter values relevant to a microgravity environment (including the Space Shuttle), as can be seen from the Introduction. Configurations involving fluids of specific interest can be investigated at greater length using this methodology.

Appendix

The form of the column vector $\hat{x}$ is given by

$$\hat{x} = (\ldots E_{n-1}, F_{n-1}, A_{n-1}, B_{n-1}, E_n, F_n, A_n, B_n, \ldots)^T \quad \text{(A1)}$$

The form of matrix $\underline{B}$ is given by

$$\begin{matrix} \ldots & -1 & 0 & 0 & & 0 \ldots \\ \ldots & 0 & -1 & 0 & & 0 \ldots \\ \ldots & 0 & 0 & -1 & & \{(\rho_{21}-1)/(1+\rho_{21})\}e^{-2k} \\ \ldots & 0 & 0 & \{(\rho_{31}-1)/(\rho_{31}+1)\} & -1 & \ldots \end{matrix} \quad \text{(A2)}$$

The form of matrix $\underline{A}$ is given by

$$\begin{matrix} \ldots 0 & 0 & 0 & 0 & in & 0 & -ke^k & ke^{-k} & 0 & 0 \ldots \\ \ldots 0 & 0 & 0 & 0 & 0 & in & -k & k & 0 & 0 \ldots \\ \ldots \beta 1 & 0 & 0 & 0 & \beta 2 & 0 & in & \beta 3 & \beta 4 & 0 \ldots \\ \ldots 0 & \beta 5 & 0 & 0 & 0 & \beta 6 & \beta 7 & in & 0 & \beta 8 \ldots \end{matrix} \quad \text{(A3)}$$

with

$$\alpha 1 = (1 + \rho_{21} + \rho_{31}), \quad \alpha 2 = (1 - \rho_{21})/(1 + \rho_{21})$$

$$\alpha 3 = (1 - \rho_{31})/(1 + \rho_{31}), \quad \alpha 4 = (1 + \rho_{21})$$

$$\alpha 5 = (1 + \rho_{31}), \quad \beta 1 = (Fr/2)e^{-k}\alpha 2$$

$$\beta 2 = (Fr/3Bo_2)k^2 e^{-k}\alpha 1/\alpha 4, \quad \beta 3 = (in)e^{-2k}\alpha 2$$

$$\beta 4 = (Fr/2)e^{-k}\alpha 2, \quad \beta 5 = (Fr/2)\alpha 3$$

$$\beta 6 = -(Fr/3Bo_3)k^2\alpha 1/\alpha 5, \quad \beta 7 = (in)\ \alpha 3$$

$$\beta 8 = (Fr/2)\alpha 3$$

Acknowledgments

This work was performed as part of Project JOVE (NAG8-149) for NASA Marshall Spaceflight Center. The authors would like to thank F. Leslie, N. Ramachandran, and C. M. Winter for helpful discussions.

References

[1]Ramachandran, N., and Winter, C. M., "The Effects of G-Jitter and Surface Tension Induced Convection on Float Zones," AIAA Paper 90-0654, Jan. 1990.

[2]Walter, H., *Fluid Sciences and Materials Sciences in Space: A European Perspective*, 1st ed., Springer-Verlag, New York, 1987, pp. 2–13.

[3]Benjamin, T. B., and Ursell, F., "The Stability of the Plane Free Surface of a Liquid in Vertical Periodic Motion," *Proceedings of the Royal Society of London*, Vol. A225, No. 1163, 1954, pp. 505–515.

[4]Gu, X. M., Sethna, P. M., and Narain, N., "On Three-Dimensional Nonlinear Subharmonic Resonant Surface Waves in a Fluid: Part 1—Theory," *Journal of Applied Mechanics*, Vol. 55, No. 1, 1988, pp. 213–219.

[5]Jacqmin, D., and Duval, W. M., "Instabilities Caused by Oscillating Accelerations Normal to a Viscous Fluid-Fluid Interface," *Journal of Fluid Mechanics*, Vol. 196, 1988, pp. 495–511.

[6]Hasewaga, E., "Waves on the Interface of Two Liquid Layers in Vertical Periodic Motion," *Bulletin of the JSME*, Vol. 26, No. 211, 1983, pp. 51–56.

[7]Drazin, P. G., and Reid, W. H., *Hydrodynamic Stability*, 1st ed., Cambridge University Press, London, England, UK, 1982, pp. 353–363.

[8]Kaufman, L., "The LZ Algorithm to Solve the Generalized Eigenvalue Problem," *SIAM Journal of Numerical Analysis*, Vol. 11, No. 5, 1974, pp. 997–1024.